Optimising finite-time photon extraction from emitter-cavity systems

W. J. Hughes[1,*], J. F. Goodwin[2], and P. Horak[1]

[1] Optoelectronics Research Centre, University of Southampton, Southampton SO17 1BJ, UK
[2] Department of Physics, University of Oxford, Clarendon Laboratory, Parks Rd, Oxford, OX1 3PU, UK
[*] w.j.hughes@soton.ac.uk

Abstract: We develop methods to find the limits to finite-time single photon extraction from emitter-cavity systems. We first establish analytic upper and lower bounds on the maximum extraction probability from a canonical Λ-system before developing a numeric method to optimise generic output probabilities from Λ-systems generalised to multiple ground states. We use these methods to study the limits to finite-time photon extraction and the wavepackets that satisfy them, finding that using an optimised wavepacket ranging between a sinusoidal and exponentially decaying profile can considerably reduce photon duration for a given extraction efficiency. We further optimise the rates of quantum protocols requiring emitter-photon correlation to obtain driving-independent conclusions about the effect of system parameters on success probability. We believe that these results and methods will provide valuable tools and insights for the development of cavity-based single photon sources combining high efficiency and high rate.

1. Introduction

Single quantum emitters coupled to optical cavities have constituted a central platform for studying the interaction of light and matter [1–3], and moreover present a possible implementation for many quantum information processes, including photon-photon gates [4] and generating long-range interaction between matter-based qubits [5–7]. A broad class of applications, such as photonic information processing [8], quantum networking [9, 10], or networked modular quantum computation [11], could utilise emitter-cavity systems to produce single photons for the required protocols. The probability of photon extraction is typically of central importance, affecting the rate of heralded protocols [12, 13] and the fidelity of deterministic ones [14].

There are several different approaches to produce single photons. To achieve fast extraction, one can directly excite the emitter [15], but to approach the ultimate bound to photon extraction probability of $2C/(2C+1)$, determined solely by the cooperativity C [16–18], cavity-assisted Raman transitions [19–21], or vSTIRAP [22] are commonly used. However, the photon production duration is typically much greater than direct excitation [21, 23] to reduce excited state population [24] or maintain adiabatic following [25] respectively. In quantum information applications, this increased photon duration leads not just to ultimately slower information processing, but increased decoherence of quantum information stored elsewhere during photon production [26–28] and increased photonic losses in the longer fibre delay lines [29]. It is thus crucial to understand how to achieve both high efficiency and high rate photon extraction from emitter-cavity systems.

In this work, we develop analytical and numerical approaches to find the limits set by system parameters on high-probability high-rate photon extraction, and how to saturate these limits. In Sec. 2, we develop upon previous approaches linking photon extraction probabilities to wavepacket shape [18, 30] to analytically optimise these wavepackets and set upper and lower bounds on the maximum emission probability for a given production time. In Sec. 3, we build upon these ideas to develop a numeric procedure that can optimise a variety of probabilities, including the emission probability, for generalised versions of Λ-systems with multiple ground states. Finally, in Sec. 4, we use these tools to investigate the limits to finite-time photon extraction, and the photon wavepackets that satisfy them, before discussing protocols requiring emitter-photon

correlations, taking remote entanglement generation [31] as a case study. Our approach of optimising the photon wavepacket directly is driving-independent, lending it complementary advantages to approaches that calculate dynamics directly from the driving pulse [32,33], notably avoiding local optima in the selected driving parametrisation or ansatzes in the driving form.

Lastly, photon extraction and absorption, though not direct time reversals of each other, are linked by time reversal [34], with the efficiency of extraction matching that of absorption for time-reversed control drives and wavepacket profiles [35]. Our results for photon extraction will therefore correspond to analogous results for photon absorption, on which there is extensive literature [35–38], but to avoid confusion, we will discuss only photon extraction contexts.

2. Three level Λ-system

2.1. Model

The model we use for the emitter-cavity photon-generation system is the canonical Λ-type emitter coupled to a single cavity mode. The emitter level structure contains two ground states, $|u\rangle$ and $|g\rangle$, which are both coupled by electromagnetic transitions to an excited state $|e\rangle$ which decays via spontaneous emission to any mode except the single cavity mode with amplitude decay rate γ. The emitter couples to a single cavity mode, whose Hilbert space contains only the vacuum state $|0\rangle$ and the single photon state $|1\rangle$. The cavity field amplitude decay rate is κ. In real systems, this decay rate comprises a 'useful' decay rate through the desired partially-transmissive mirror κ_T, and a 'parasitic' decay rate κ_I which includes other losses such as scattering, absorption, and diffraction. To reduce the number of variables, we assume $\kappa_I = 0$ and therefore $\kappa_T = \kappa$. However, the coherent dynamics of the system are determined solely by κ, therefore all future results will hold for cavities with $\kappa_I \neq 0$ provided any output probabilities are attenuated by $\kappa_T/(\kappa_T + \kappa_I)$. The coupling between the excited atomic state with an empty cavity $|e, 0\rangle$, and the ground state with an occupied cavity $|g, 1\rangle$ is, by convention, g, with detuning Δ_e of the $|e\rangle \rightarrow |g\rangle$ emitter transition frequency from the cavity mode frequency. A diagram of the system is depicted in Fig. 1.

In a general photon production process, the cavity is initially vacant, the emitter is prepared in state $|u\rangle$, and a time-dependent driving pulse $\Omega(t)$ is applied to transfer population, via $|e, 0\rangle$, to $|g, 1\rangle$. The single photon then leaks out of the cavity and is collected. This Λ-system model is sufficiently general to describe photon production through direct excitation, cavity-assisted Raman transition or vSTIRAP through appropriate choices of the driving pulse $\Omega(t)$ and detuning Δ_e [16]. Regardless of the driving method chosen, the maximum photonic output of the system is

$$\begin{aligned} P_\kappa^{(a)} &= \frac{2C}{2C+1}, \\ C &= \frac{g^2}{2\kappa\gamma}, \end{aligned} \tag{1}$$

where the dimensionless C is the cooperativity [16]. This performance is achieved in the adiabatic (i.e. infinite extraction time) limit, and the goal of this manuscript is to determine similar limits for non-adiabatic timescales.

The coherent Hamiltonian for this model is

$$H = \Delta_u \left|u, 0\right\rangle\!\left\langle u, 0\right| + \Delta_e \left|e, 0\right\rangle\!\left\langle e, 0\right| + \left[-i\Omega^* \left|u, 0\right\rangle\!\left\langle e, 0\right| + \text{h.c.}\right] + \left[ig \left|e, 0\right\rangle\!\left\langle g, 1\right| + \text{h.c.}\right], \tag{2}$$

where the factor of the imaginary unit i before g is made for algebraic convenience. The nominal detuning of the initial state from Raman resonance with $|g, 1\rangle$ is Δ_u, which is usually set to zero in monochromatic driving schemes.

The system dynamics also feature two incoherent decay channels, spontaneous emission from the excited state and decay of the cavity mode, which may be included in the model by using the

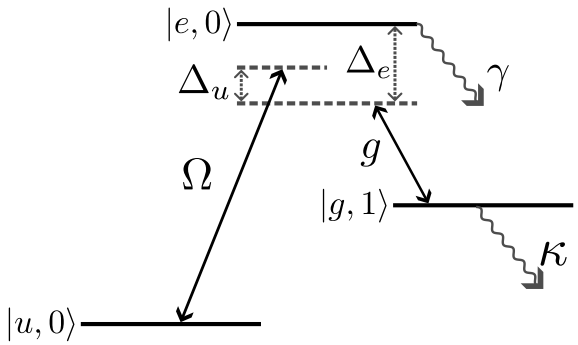

Fig. 1. The level scheme for the Λ-emitter coupled to a single cavity mode. The Hilbert space contains three levels that are all tensor products of the emitter's electronic state and the cavity mode Fock state. These levels are the initial emitter state with no cavity photon $|u,0\rangle$, an excited emitter state with no cavity photon $|e,0\rangle$, and a final emitter state with a cavity photon $|g,1\rangle$. The excited state and final state are coupled by the cavity coupling g, with the excited state detuned from resonance with the cavity by Δ_e. The initial and excited state are coupled by a laser field with complex time-dependent coupling Ω. The detuning of the laser field from Raman resonance with the cavity is Δ_u, although this is only nominal as the laser field can be adjusted to include an arbitrary detuning in its time dependence. The excited state amplitude decays at a rate γ due to spontaneous emission, and the cavity state amplitude at a rate κ due to field loss from the cavity.

master equation. However, for emitter-cavity systems operating as photon sources, the dynamics are only relevant if the cavity emits a photon. This means that, on the assumption that no decay process can be followed by subsequent cavity decay, a simpler non-Hermitian Hamiltonian

$$H^{\mathrm{NH}} = H - i\gamma\,|e,0\rangle\langle e,0| - i\kappa\,|g,1\rangle\langle g,1|\,, \tag{3}$$

can be used. The assumption that no decay process is followed by cavity decay is typically valid for cavity decay itself (provided the state $|g\rangle$ is stable on the timescale of the photon production process). However, spontaneous emission followed by cavity decay can also occur. This causes the emission of a probabilistic mixture of photon wavepackets, known as temporal mixing, which reduces the coherence and indistinguishability of photon wavepackets [39], resulting in major fidelity reductions for certain quantum protocols [40,41]. Choosing a Λ-system where the excited state decay has a low branching ratio to the initial state $|u\rangle$ strongly mitigates this effect [42]. Because temporal mixing errors can be so destructive to the coherence of the output wavepacket, we assume that the Λ-system has been chosen such that temporal mixing is negligible and, therefore, that the non-Hermitian approach is applicable. In the case that temporal mixing is not negligible, the results we derive maximise the probability of an emission event that is not preceded by a spontaneous emission event.

Finally, we note that recent work [43] has proposed the use of multiple excited states to realise the reduced temporal mixing found in systems with low branching ratios to $|u\rangle$, but in systems that do not naturally have that structure. At the end of Sec. 2.2, we discuss how our results also apply to these systems.

2.2. Bounded optimisation approach

Using the non-Hermitian approach, our analysis initially follows Goto (2019) [16] to link the probabilities of cavity emission and spontaneous emission to the photon shape, and then, as suggested in Vasilev (2010) [18], optimises this shape to yield the maximum output.

We begin by expressing explicitly the non-Hermitian Hamiltonian Eq. (3)

$$
\begin{aligned}
|\Psi(t)\rangle &= \alpha_u |u,0\rangle + \alpha_e |e,0\rangle + \alpha_g |g,1\rangle, \\
\dot{\alpha_u} &= -i\Delta_u \alpha_u - \Omega^* \alpha_e, \\
\dot{\alpha_e} &= -(\gamma + i\Delta_e)\alpha_e + \Omega\alpha_u + g\alpha_g, \\
\dot{\alpha_g} &= -\kappa\alpha_g - g\alpha_e,
\end{aligned}
\tag{4}
$$

where $|\Psi(t)\rangle$ is the wavefunction of the emitter-cavity system. Rearrangement of the last relation yields

$$
\alpha_e = -\frac{1}{g}\left(\kappa\alpha_g + \dot{\alpha_g}\right), \tag{5}
$$

which expresses the wavefunction component of $|e,0\rangle$ through the component in the state $|g,1\rangle$.

Throughout the photon generation process, the three level system with two decay channels has probabilities of occupation split across five categories: $P_u(t)$, $P_e(t)$, and $P_g(t)$ are the occupation probabilities of states $|u,0\rangle$, $|e,0\rangle$, and $|g,1\rangle$ at time t respectively, $P_\gamma(t)$ is the probability that there has been decay by spontaneous emission by time t, and $P_\kappa(t)$ is the probability that there has been photonic decay from the cavity by time t.

These probabilities, with the exception of P_u, can be written using Hermitian integrals of the form

$$
I_{(nm)}(t) = \int_0^t \left(\overset{n\cdot}{\alpha_g}\overset{m\cdot *}{\alpha_g} + \overset{m\cdot}{\alpha_g}\overset{n\cdot *}{\alpha_g}\right) dt, \tag{6}
$$

where $n\cdot$ is a shorthand for n copies of $\cdot$ to indicate n time derivatives. Using this notation, the probabilities are

$$
\begin{aligned}
P_\kappa(t) &= \kappa I_{(00)}(t), \\
P_g(t) &= I_{(10)}(t), \\
P_\gamma(t) &= \frac{\gamma\kappa^2}{g^2} I_{(00)}(t) + \frac{2\gamma\kappa}{g^2} I_{(10)}(t) + \frac{\gamma}{g^2} I_{(11)}(t), \\
P_e(t) &= \frac{\kappa^2}{g^2} I_{(10)}(t) + \frac{\kappa}{g^2} I_{(20)}(t) + \frac{\kappa}{g^2} I_{(11)}(t) + \frac{1}{g^2} I_{(21)}(t) + \frac{1}{g^2}\left|\dot{\alpha_g}(0)\right|^2, \\
P_u(t) &= 1 - P_\kappa(t) - P_g(t) - P_\gamma(t) - P_e(t),
\end{aligned}
\tag{7}
$$

where the derivations are given in Supplement 1 Sec. 1.

Assuming that any driving pulse $\Omega(t)$ can be applied, the $\alpha_e(t)$ required to produce a desired $\alpha_g(t)$ is possible provided there is sufficient probability $P_u(t)$ at all times to control the dynamics. In particular, an unphysical wavepacket $\alpha_g(t)$ will cause $P_u(t)$, which is calculated through probability conservation, to drop below zero at some time during the process. Therefore, a physical solution should satisfy $P_u(t) \geq 0,\ 0 \leq t \leq T$, with the optimal solution having $P_u(t_{\max}) = 0$ for some time $t_{\max}$ during the process (see [18, 30] for previous uses of this condition). This condition is troublesome to impose analytically as it applies a separate constraint for every time during photon production. Instead, we demand that no probability remains in the initial or excited state at the end of the process ($P_u(T) + P_e(T) = 0$), which can be simply enforced. This 'upper bound constraint' is less restrictive than the true constraint in the sense that any dynamics satisfying the true constraint has output probability less than or equal to some dynamics satisfying the upper bound constraint. This can be seen by noting that a solution satisfying the true constraint must satisfy $P_u(T) + P_e(T) \geq 0$, where the inequality can be converted to the equality of the upper bound constraint by uniformly increasing the scale of α_g, and therefore increasing the output probability. Solutions derived under the upper bound constraints therefore constitute upper bounds to the optimum photon extraction probabilities, and will be denoted with a superscript (U).

The constraint $P_u(T) + P_e(T) = 0$ can be rewritten

$$1 = P_\kappa^{(U)}(T) + P_g^{(U)}(T) + P_\gamma^{(U)}(T), \tag{8}$$

as the five probabilities must always sum to unity. This yields a final output probability

$$\begin{aligned} P_\kappa^{(U)}(T) &= \frac{1}{1+m}, \\ m &= \frac{P_g^{(U)}(T) + P_\gamma^{(U)}(T)}{P_\kappa^{(U)}(T)} \equiv \frac{F}{G}, \end{aligned} \tag{9}$$

where m is a scalar determined by the shape of the photon wavepacket and F and G are functionals of α_g introduced for notational convenience.

As seen from Eq. (9), the optimum output probability occurs when m is minimised. To minimise m, assume that α_g changes by $\delta\alpha_g$, causing a change in F (G) of δF (δG). The condition that m is an extremum gives $\delta F/\delta G = F/G$. Now define a shape functional

$$S_q = P_g^{(U)}(T) + P_\gamma^{(U)}(T) - qP_\kappa^{(U)}(T) = F - qG, \tag{10}$$

for a general scalar q. Extrema of S_q satisfy $\delta F/\delta G = q$. Therefore, the procedure to find extrema of m with respect to changes in the photon shape α_g is a two-stage process: first, find the extrema of S_q for all q and second, check that $q = F/G = m$. In other words, stationary solutions must satisfy

$$\begin{aligned} \delta S_q &= 0, \\ q &= \frac{F}{G} \equiv m, \end{aligned} \tag{11}$$

simultaneously, and the optimum solution is that with the smallest q. To satisfy the first condition of Eq. (11), we find stationary S_q according to

$$\begin{aligned} S_q &= \int_0^T L_q \, dt, \\ L_q &= \left(\frac{\gamma\kappa^2}{g^2} - q\kappa\right)\alpha_g\alpha_g^* + \left(1 + \frac{2\gamma\kappa}{g^2}\right)\dot{\alpha_g}\alpha_g^* + \frac{\gamma}{g^2}\dot{\alpha_g}\dot{\alpha_g}^* + \text{c.c.}, \end{aligned} \tag{12}$$

where c.c. is a shorthand for complex conjugate, and the 'effective Lagrangian' L_q has been written explicitly using Eq. (7). Using the Euler-Lagrange equations to minimise this functional

$$\frac{\partial L_q}{\partial \alpha_g} = \frac{d}{dt}\left(\frac{\partial L_q}{\partial \dot{\alpha_g}}\right), \tag{13}$$

produces a differential equation

$$\ddot{\alpha_g} + \kappa^2\left(2Cq - 1\right)\alpha_g = 0, \tag{14}$$

for the wavefunction of the cavity mode. This equation has two types of solution. If $q < 1/(2C)$, the solutions are hyperbolic functions, whereas in the opposite case, they are trigonometric functions. It is shown in Supplement 1 Sec. 2 (and could also be inferred directly from Eq. (1)) that the hyperbolic solution produces $m \geq 1/(2C)$, and therefore can never satisfy the second constraint of Eq. (11). This means that the required $q \geq 1/(2C)$, resulting in trigonometric solutions. Setting the boundary condition that the cavity is vacant at the start of the process gives

$$\begin{aligned} \alpha_g(t) &= A\sin\left(\omega_q t\right), \\ \omega_q^2 &= \kappa^2\left(2Cq - 1\right), \end{aligned} \tag{15}$$

where A is a free parameter that can be set to adjust the sum of probabilities. The probabilities from Eq. (7) can be calculated explicitly using this solution:

$$\begin{aligned}
P_\kappa(t) &= A^2\left(\kappa t - \frac{\kappa}{2\omega_q}\sin\left(2\omega_q t\right)\right),\\
P_g(t) &= A^2\sin^2\left(\omega_q t\right),\\
P_\gamma(t) &= \frac{P_\kappa(t)}{2C} + A^2\left\{\frac{1}{C}\sin^2(\omega_q t) + \frac{\omega_q^2}{\kappa^2}\frac{1}{2C}\left(\kappa t + \frac{\kappa}{2\omega_q}\sin\left(2\omega_q t\right)\right)\right\},\\
P_e(t) &= A^2\left(\frac{\omega_q}{g}\cos\left(\omega_q t\right) + \frac{\kappa}{g}\sin\left(\omega_q t\right)\right)^2.
\end{aligned} \tag{16}$$

Substituting these results at time T into the second condition of Eq. (11) ($q = F/G$) results in

$$\cos\left(2\omega_q T\right) - \frac{2\omega_q}{2\kappa(1+C)}\sin\left(2\omega_q T\right) = 1. \tag{17}$$

This equation has many solutions, however, when satisfied, $q = F/G = m$, and therefore, to minimise m, the solution of interest has the minimum q and therefore ω_q. There is a solution at $\omega_q = \pi/T$, corresponding to a cavity wavefunction α_g (and thus photon wavepacket) of sinusoidal amplitude, beginning at zero and first returning to zero again at time T. However, there is a better solution at a lower q, which retains a sinusoidal shape, but with a slower temporal frequency ω_q so that the photon does not fully close by time T.

Thus the upper bound can be summarised

$$\begin{aligned}
1 &= \cos(2\omega_m T) - \frac{2\omega_m}{2\kappa(1+C)}\sin(2\omega_m T),\\
m &= \frac{1}{2C}\left(\left(\frac{\omega_m}{\kappa}\right)^2 + 1\right),\\
P_\kappa^u &= \frac{1}{1+m},
\end{aligned} \tag{18}$$

where m is taken as the smallest value to satisfy the first equation, which must be solved numerically. The same optimisation could have been performed using Lagrange multipliers, but in that approach it is less clear which stationary solution is the global minimum and it is not emphasised so strongly that the optimisation performed optimises the photon shape.

The upper bound is an output optimised under the condition that the population remaining in the cavity P_g, emitted spontaneously P_γ and decayed through the cavity P_κ sum to unity at time T. This is less restrictive than the true condition that these probabilities, in addition to the probability in the excited state P_e reaches unity at some point in the process. We obtain a lower bound to the output probability P_κ^l by assuming the photon retains the same amplitude profile, but reduced in scale to satisfy the true probability constraint. This is a lower bound because the photon shape has not been optimised for the true constraint.

A potential objection against the validity of these sinusoidal solutions is that the initial occupation of the excited state $|e,0\rangle$ is non-zero, whereas the problem stipulates that the system is prepared in state $|u,0\rangle$. However, provided arbitrary driving is possible, probability can be transferred infinitely quickly from $|u,0\rangle$ to $|e,0\rangle$ at the beginning of the process. This means that the lower bound photon solution *can* be produced from an initial state of $|u,0\rangle$ in a time only infinitesimally longer that T, and therefore the bounds apply unchanged in the case that the excited state is initially vacant. Indeed the ability to set a non-zero occupation of $|e,0\rangle$ at time $t = 0$ is advantageous because it means that the effect of arbitrarily strong driving at the initial time can be captured without requiring these troublesome dynamics be modelled explicitly.

Finally, it is worth noting that, while the bounds have been derived for a Λ-system, they are applicable to a wider class of systems. This is because the level structure through which wavefunction amplitude is delivered to the excited state is not relevant provided it does not restrict the possible $\alpha_e(t)$. In particular, as mentioned in Sec. 2, a recent paper [43] has suggested the use of two excited states to reduce photon indistinguishability due to temporal mixing. Provided both of the driving fields used in that scenario can realise arbitrary amplitude profiles such that the occupation of the additional excited state is always negligible, a very similar derivation to the above can be made for those systems. This finds identical bounds to the Λ system, which extends to finite time the equivalent adiabatic result described in that paper.

The upper and lower bounds described in this section can be readily calculated, but before those results are presented in Sec. 4, the numerical method will be developed.

3. Numerical Method for Generalised Λ-systems

3.1. Defining the system

The results presented in Sec. 2.2 set useful bounds on the limits of performance for Λ-systems, but there are benefits to a more flexible numeric approach. Firstly, while we know that the true limit to performance for the Λ-system lies between the upper and lower bounds found in Sec. 2.2, we do not know where between these bounds the limit lies. Secondly, real emitter level structures often contain additional decay channels near-resonant with the cavity modes, which, in atom or ion emitters, would typically be to alternative sublevels within the fine or hyperfine structure. Often, these additional levels must be included to make simulations consistent with experiment [32, 33, 44], and thus would ideally feature in our model. Finally, this extra structure can also be utilised to perform protocols which produce single photons entangled with their emitter [13, 45], meaning that the ability to model systems with additional ground states is essential to determine the limits of these protocols.

The ideas presented in Sec. 2.2 inspire a numerical method presenting these benefits. The systems modelled again contain a single initial state $|u, 0\rangle$ and excited state $|e, 0\rangle$, but now potentially multiple distinct states with occupied cavity modes $\left|g_j, 1_j\right\rangle$ for $1 \leq j \leq j_M$, where j_M is the number of emitter transitions to which the cavity couples. The states $\left|g_j, 1_j\right\rangle$, henceforth known as 'emitter-occupied cavity states', are each coupled to the excited state with respective coupling rate g_j. For atomic emitter-cavity applications using dipole-allowed transitions there may be three emitter-occupied cavity states for the three possible angular momentum transitions (π or $\sigma_\pm$). However, the number of emitter-occupied cavity states is reduced if a decay is not allowed by atomic selection rules or if the cavity axis lies along the magnetic field and the π decay is not supported, or increased if multiple state manifolds are close to resonance, for example due to hyperfine structure. Note that while the emitter-occupied cavity states $\left|g_j, 1_j\right\rangle$ should be mutually orthogonal, neither the ground atomic states $\left\{\left|g_j\right\rangle\right\}$ nor occupied photon modes (whose single-occupancy states are denoted $\left|1_j\right\rangle$) need be mutually orthogonal. For non-birefringent cavities (where the two orthogonal polarisation modes associated with a spatial profile are degenerate), the most natural choice is to use a mutually orthogonal basis of atomic eigenstates $\left\{\left|g_j\right\rangle\right\}$, and define the corresponding photon states $\left|1_j\right\rangle$ through the cavity interaction. The level scheme is shown in Fig. 2 for an example of two emitter-occupied cavity states. The equations of motion are

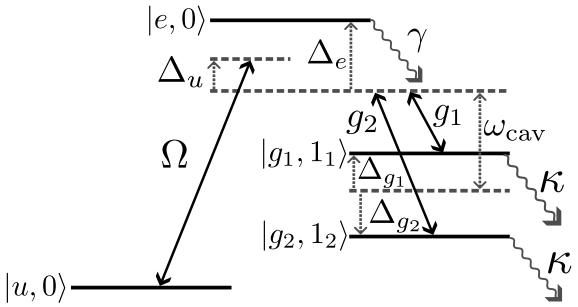

Fig. 2. The level scheme for the generalised Λ-system coupled to a cavity mode, here depicted with two emitter-occupied cavity states. Compared to Fig. 1, the Hilbert space of the system now contains an arbitrary number of emitter-occupied cavity states (indexed by j) with cavity mode occupation $|g_j, 1_j\rangle$ coupled to the excited state with respective coupling g_j. The emitter-occupied cavity states are each detuned from a nominal central energy level by detuning Δ_{g_j} from which the excited state is itself detuned by Δ_e when including the cavity photon energy ω_{cav}.

$$
\begin{aligned}
|\Psi(t)\rangle &= \alpha_u |u,0\rangle + \alpha_e |e,0\rangle + \sum_{j=1}^{j_M} \alpha_{g_j} |g_j, 1_j\rangle, \\
\dot{\alpha_u} &= -i\Delta_u \alpha_u - \Omega^* \alpha_e, \\
\dot{\alpha_e} &= -(\gamma + i\Delta_e)\alpha_e + \Omega\alpha_u + \sum_{j=1}^{j_M} g_j \alpha_{g_j}, \\
\dot{\alpha_{g_j}} &= -(\kappa + i\Delta_{g_j})\alpha_{g_j} - g_j \alpha_e \;\; \forall j \; 1 \le j \le j_M,
\end{aligned}
\tag{19}
$$

where Δ_{g_j} is the detuning of emitter-occupied cavity state $|g_j, 1_j\rangle$ from an arbitrary reference level, which, for numerical convenience, is best chosen near the centre of the manifold of emitter-occupied cavity states.

The difficulty with optimising the outputs of this system is that, given appropriate boundary conditions, specifying an output wavefunction (for example $\alpha_{g_1}(t)$) will intrinsically specify all other $\alpha_{g_j}(t)$ as occupied cavity-states couple only to one excited state $|e,0\rangle$. This interdependence is not straightforward to treat in the time domain as it involves both wavefunction terms and their time derivatives.

Instead, the wavefunction coefficients $\alpha_{g_j}(t)$ can be specified as a sum

$$
\begin{aligned}
\alpha_{g_j}(t) &= \frac{1}{\sqrt{T_b}} \sum_n C_n^{(j)} e^{i\omega_n t}, \\
\omega_n &= \frac{2\pi}{T_b} n,
\end{aligned}
\tag{20}
$$

of Fourier coefficients $C_n^{(j)}$ across a time domain of length T_b which, as the photon wavefunctions start at zero amplitude but are not necessarily zero at T, must exceed T. The time-domain function $\alpha_{g_j}(t)$ can then be specified equivalently as a column vector in Fourier space,

$$
\overrightarrow{\alpha_{g_j}^F} = (..., C_{-1}^{(j)}, C_0^{(j)}, C_1^{(j)}, C_2^{(j)}, ...)^T. \tag{21}
$$

The equations of motion Eq. (19) relate the n$^{\mathrm{th}}$ Fourier coefficient of the k$^{\mathrm{th}}$ emitter-occupied cavity state $|g_k, 1_k\rangle$ to the same coefficient of the j$^{\mathrm{th}}$ emitter-occupied cavity state $|g_j, 1_j\rangle$ through

$$C_n^{(k)} = \frac{g_k}{g_j}\frac{\kappa + i(\omega_n + \Delta_{g_j})}{\kappa + i(\omega_n + \Delta_{g_k})} C_n^{(j)} \equiv f_n^{(j\to k)} C_n^{(j)}. \tag{22}$$

Thus any output probability can be maximised with only the vector $\overrightarrow{\alpha^F_{g_j}}$ as a variable because the wavefunction components in the remainder of the emitter-occupied cavity states may be automatically encoded in the relations of Eq. (22)

3.2. Calculating Probabilities

To maximise a desired output probability of the system, a selection of probabilities must be determined. These probabilities are

- $P_{\kappa_j}(t)$: The probability that a photon is emitted via $\left|g_j, 1_j\right\rangle$ before time t.
- $P_\gamma(t)$: The probability of spontaneous emission before time t.
- $P_{g_j}(t)$: The probability that state $\left|g_j, 1_j\right\rangle$ is occupied at time t.
- $P_e(t)$: The probability that $|e, 0\rangle$ is occupied at time t.

These probabilities can all be written as expectation values of matrices $\hat{P_\zeta}$ with vector $\overrightarrow{\alpha^F_{g_j}}$ such that

$$P_\zeta(t) = \overrightarrow{\alpha^F_{g_1}}^\dagger \cdot \hat{P_\zeta}(t) \cdot \overrightarrow{\alpha^F_{g_1}}, \tag{23}$$

for generic probability P_ζ. Derivations of these matrices are presented in Supplement 1 Sec. 3, resulting in

$$\begin{aligned}
\hat{P_{\kappa_j}}_{n',n}(t) &= 2\kappa (f_{n'}^{(1\to j)})^* \hat{V}_{n',n}(t) f_n^{(1\to j)}, \\
\hat{P_{g_j}}_{n',n}(t) &= (f_{n'}^{(1\to j)})^* (\exp\{i(\omega_n - \omega_{n'})t\}) f_n^{(1\to j)}, \\
\hat{P_\gamma}_{n',n}(t) &= \frac{2\gamma}{g_1^2}\left[\kappa^2 + \Delta_{g_1}^2 + i\kappa(\omega_n - \omega_{n'}) + \Delta_{g_1}(\omega_n + \omega_{n'}) + \omega_n\omega_{n'}\right]\hat{V}_{n',n}(t), \\
\hat{P_e}_{n',n}(t) &= \frac{1}{g_1^2 T_b}\left[\kappa^2 + \Delta_{g_1}^2 + i\kappa\left(\omega_n - \omega_{n'}\right) + \Delta_{g_1}\left(\omega_n + \omega_{n'}\right) + \omega_n\omega_{n'}\right]\exp\left\{i(\omega_n - \omega_{n'})t\right\},
\end{aligned} \tag{24}$$

where

$$\hat{V}_{n',n}(t) = \left.\begin{array}{ll} \dfrac{2}{T_b\left(\omega_n - \omega_{n'}\right)}\sin\left(\dfrac{1}{2}\left(\omega_n - \omega_{n'}\right)t\right)\exp\left(\dfrac{1}{2}i\left(\omega_n - \omega_{n'}\right)t\right), & \omega_n \neq \omega_{n'}, \\ \dfrac{t}{T_b}, & \omega_n = \omega_{n'}. \end{array}\right\} \tag{25}$$

3.3. Enforcing the Initial Vacancy of emitter-occupied cavity states

The solution must satisfy the constraint that there is no cavity occupation at $t = 0$. Consider enforcing this condition on just the $j = 1$ emitter-occupied cavity state.

$$0 = \alpha_{g_1}(0) = \frac{1}{\sqrt{T_b}}\sum_n C_n^{(1)}. \tag{26}$$

In the Fourier domain, this constraint is encoded

$$\begin{aligned}
\overrightarrow{\phi_1^F}^\dagger \cdot \overrightarrow{\alpha^F_{g_1}} &= 0, \\
\left(\overrightarrow{\phi_1^F}^\dagger\right)_n &= 1.
\end{aligned} \tag{27}$$

Equivalent conditions for the other emitter-occupied cavity states lead to a set of j_M conditions,

$$\begin{aligned} \overrightarrow{\phi_j^F}^\dagger \cdot \overrightarrow{\alpha_{g_1}^F} &= 0 \ \forall j, \\ \left(\overrightarrow{\phi_j^F}^\dagger\right)_n &= (f_n^{(1\to j)})^*. \end{aligned} \tag{28}$$

The j_M vectors $\overrightarrow{\phi_j^F}$ define a j_M^d-dimensional subspace in which a valid solution vector $\overrightarrow{\alpha_{g_1}^F}$ should not lie, where $j_M^d \leq j_M$ is the number of non-degenerate emitter-occupied cavity states. We use Gram Schmidt orthogonalisation to produce a basis in which the final j_M^d states span this subspace, along with a matrix $\hat{U}$ that transforms a state in the Fourier basis to this basis. Additionally, we define the projector $\hat{\Pi}_{j_M^d}$ which removes the last j_M^d components of a vector, and the reverse projector $\tilde{\hat{\Pi}}_{j_M^d}$ that takes a reduced vector and appends j_M^d coefficients with value zero. Any Fourier vector $\overrightarrow{\alpha_{g_1}^F}$ can now be projected to a solution that satisfies the initial conditions

$$\overrightarrow{\alpha_{g_1}^P} = \hat{\Pi}_{j_M^d} \hat{U} \overrightarrow{\alpha_{g_1}^F}, \tag{29}$$

where $\overrightarrow{\alpha_{g_1}^P}$ is expressed as coefficients in the 'projected' basis, to which the superscript P refers. Probability matrices

$$\hat{P_\zeta^P} = \hat{\Pi}_{j_M^d} \hat{U} \hat{P_\zeta} \hat{U}^\dagger \tilde{\hat{\Pi}}_{j_M^d}, \tag{30}$$

are then written in the new projected basis where ζ is a generic index that specifies the probability, with these projected matrices again labelled by superscript P. Within the projected basis, every state automatically satisfies the initial conditions, and therefore these conditions need not be explicitly enforced during optimisation.

3.4. Normalising Probabilities

The (projected) matrix for total probability not in the initial state at time t

$$\hat{P_{\overline{u}}^P}(t) = \sum_{j=1}^{j_M} \left(\hat{P_{\kappa_j}^P}(t) + \hat{P_{g_j}^P}(t) \right) + \hat{P_\gamma^P}(t) + \hat{P_e^P}(t), \tag{31}$$

can be calculated from other probability matrices. As in the analysis of Sec. 2.2, a photon shape is possible if the total probability not in the initial state remains below unity for all times. We therefore define normalised probabilities as those found when the photon amplitude is re-scaled to the maximum that can satisfy this constraint. The normalised probability corresponding to a generic probability $P_\zeta(t)$ is

$$P_\zeta^N(t) = \frac{\overrightarrow{\alpha_{g_1}^P}^\dagger \cdot \hat{P_\zeta^P}(t) \cdot \overrightarrow{\alpha_{g_1}^P}}{\overrightarrow{\alpha_{g_1}^P}^\dagger \cdot \hat{P_{\overline{u}}^P}(t_{\max}) \cdot \overrightarrow{\alpha_{g_1}^P}}, \tag{32}$$

where $0 \leq t_{\max} \leq T$ is the time for which $[\overrightarrow{\alpha_{g_1}^P}^\dagger \cdot \hat{P_{\overline{u}}^P}(t_{\max}) \cdot \overrightarrow{\alpha_{g_1}^P}]$ is maximised. This expression automatically normalises probabilities such that the sum of all calculated probabilities remains less than or equal to unity for the photon production process. Thus, when using normalised probabilities, the magnitude of the photon vector $\overrightarrow{\alpha_{g_1}^P}$ has no significance.

3.5. Optimising Probabilities

To optimise probabilities, we use an iterative approach. Consider optimising a generic product of probabilities

$$V = \prod_{l=1}^{l_M} P^N_{\zeta_l}(t_l), \tag{33}$$

where l_M is the order of the probability product, ζ_l specifies the probability of the term in the product labelled by l, and t_l is the time at which the probability should be evaluated. In general, a sum of such products can be desired, but this is just a trivial extension. Each cycle of an iterative procedure begins with the current solution vector $\overrightarrow{\alpha^P_{g_1}}$. This vector is modified by adding a small correction

$$\delta\overrightarrow{\alpha^P_{g_1}} = \epsilon \left[\left(\sum_{l=1}^{l_M} \hat{P^P_{\zeta_l}}(t_l) \cdot \overrightarrow{\alpha^P_{g_1}} \right) - l_M \hat{P^P_{\overline{u}}}(t_{\max}) \cdot \overrightarrow{\alpha^P_{g_1}} \right], \tag{34}$$

where ϵ is set to a randomly-chosen positive small number at each iteration to prevent the optimisation stalling and $t_{\max}$ is evaluated every iteration. This additional vector $\delta\overrightarrow{\alpha^P_{g_1}}$ lies along the gradient of V with respect to the projected solution vector $\overrightarrow{\alpha^P_{g_1}}$ under the assumption that $t_{\max}$ does not change.

3.6. Applicability to experiments

The method presented in this section finds the output wavepacket that maximises a desired probability, however, this might not be the best practical solution for two main reasons. Firstly, physically realising the optimum output requires arbitrary control over the driving field, including effectively instantaneous transfers pulses at the start of, and potentially during, the process (the method to calculate the driving pulse from a solution for $\alpha_{g_1}(t)$ is given in Supplement 1 Sec. 4). In real experiments, the possible drive pulses are typically restricted, for example by the available drive power or modulator slew rates. It is much simpler to include these restrictions in optimal control approaches that optimise the driving parameters directly. Therefore, a sequential procedure first using our approach to find the performance limits fundamental to the emitter-cavity system followed by optimal control to find a realisable drive solution with performance close to these limits may be most effective. Secondly, the usefulness of photon wavepackets for a given application is often not solely a question of their total probability. For example, for applications involving photon interference, the wavepackets would ideally offer low sensitivity to inevitable pathlength differences [46] through reasonably stable intensity and phase profiles, a criterion which is not trivial to satisfy [47]. Therefore a more general notion of photon desirability might be required. If these additional factors can be encoded as probability products, it may be possible to perform that optimisation within our framework, but again, a two-stage approach whose first step uses our method to understand the system limits may be more generally applicable.

3.7. Role of detunings

Finally, it should be noted that, at no point during the optimisation, here or for the analytical approach in Sec. 2.2, did the detunings Δ_e and Δ_u feature. Therefore, the optimised wavepacket and probability are independent of their values. For Δ_u, this is expected, because its value is only nominal as any change to its value could be compensated by the arbitrary drive pulse. However, Δ_e is a physical variable, so the conclusion that the optimum performance of these systems is unaffected by its value is not obvious, but this conclusion has been found in the adiabatic regime for photon generation [16] and storage [38], and for the generation of Gaussian wavepackets [30]. As in these cases, the driving pulse to produce the optimum performance does depend on Δ_e, even though the photon wavepacket and output probability does not.

4. Results

In this section, we will use the analytic and numeric methods developed in Sections 2.2 and 3 respectively to understand the limits of photon extraction in different scenarios. First, we will look at the Λ-system to evaluate the finite-time limits of photon extraction, the photon wavepackets that saturate these limits, and the scale of the benefits in decreased photon duration bestowed by these optimised wavepackets. Then, we focus on systems with more than one emitter-occupied cavity state, demonstrating probability maximisation of different outputs, before performing a case study on how ground-state energy separation limits the success rates of systems designed for remote entanglement. Details on how numerical parameters such as the number of Fourier basis states were chosen are given in Supplement 1 Sec. 5.

4.1. Optimum output of Λ-systems in finite time

As mentioned in Sec. 2.1, the optimum output from a Λ-system, $P_\kappa^{(a)}$ (Eq. (1)), strictly applies only in infinite time. However, recent work studying Gaussian wavepackets [30], in agreement with the numerical findings of [38], indicates that output close to $P_\kappa^{(a)}$ is achieved provided the photon timescale (T in our notation) is much greater than the 'critical time'

$$t_{\text{crit}} = \max\left(\frac{\kappa}{g^2}, \frac{1}{\kappa}\right). \tag{35}$$

This expression indicates two regimes for the ratio of g to κ, with a boundary between them at $g = \kappa$.

An alternative to trying to drive a photon on timescale T is to instantly excite the emitter to $|e, 0\rangle$ at $t = 0$ and wait for the excitation to transfer to the cavity mode and leak out to the collection. This technique produces photons quickly, but does so at an infinite-time probability

$$P_\kappa^{(e)} = \frac{\kappa}{\kappa + \gamma} P_\kappa^{(a)}, \tag{36}$$

which is below the adiabatic limit [48]. The notions of t_{crit} and $P_\kappa^{(e)}$ highlight the trade-off that practical applications must balance between the rate of photon production $1/T$ and the extraction probability $P_\kappa(t)$. We use our analytic and numerical methods to find the limits of this trade-off.

We examine these limits in Fig. 3 for three example systems with cooperativity $C = 1$, but with the ratio of κ to g chosen to sample the two regimes of t_{crit} (Eq. (35)) and the boundary between them. Examining first the comparison for different drive techniques over a range of times (Column i), the numerical result lies between the upper and lower bounds to the maximised photon extraction, which converge to $P_\kappa^{(a)}$ for $T \gg t_{\text{crit}}$ as expected. The upper and lower bounds are quite distinct for the 'bad cavity' (high κ, row a), but take similar values for $g \geq \kappa$. An instant excitation approach generally performs well at short times, but the output saturates at $P_\kappa^{(e)}$, which is particularly limiting for the parameters of row c). The linear drive curves provide an example of 'simple' driving procedures, indicating how, particularly for the parameters of row a) and b), optimisation of the output wavepacket shape can lead to much faster photon production at a given efficiency. However, the performance of linear drives does tend to the maximum output probability in the adiabatic limit $T \gg t_{\text{crit}}$, consistent with previous conclusions that photon extraction [16] and absorption [36] probabilities reach this limit in infinite time regardless of wavepacket shape.

Columns ii) and iii) show the system occupations and photon wavepackets respectively for case studies taking $T = 2.5t_{\text{crit}}$ respectively. Here we see that, in the case that $g \gg \kappa$ (row c), the optimised photon wavepacket has a very similar shape to the upper and lower bounds. However, as κ increases (row b and then a), the wavepacket shape deviates significantly from the sinousoid form, instead exhibiting a sharp rise followed by a prolonged exponential decay.

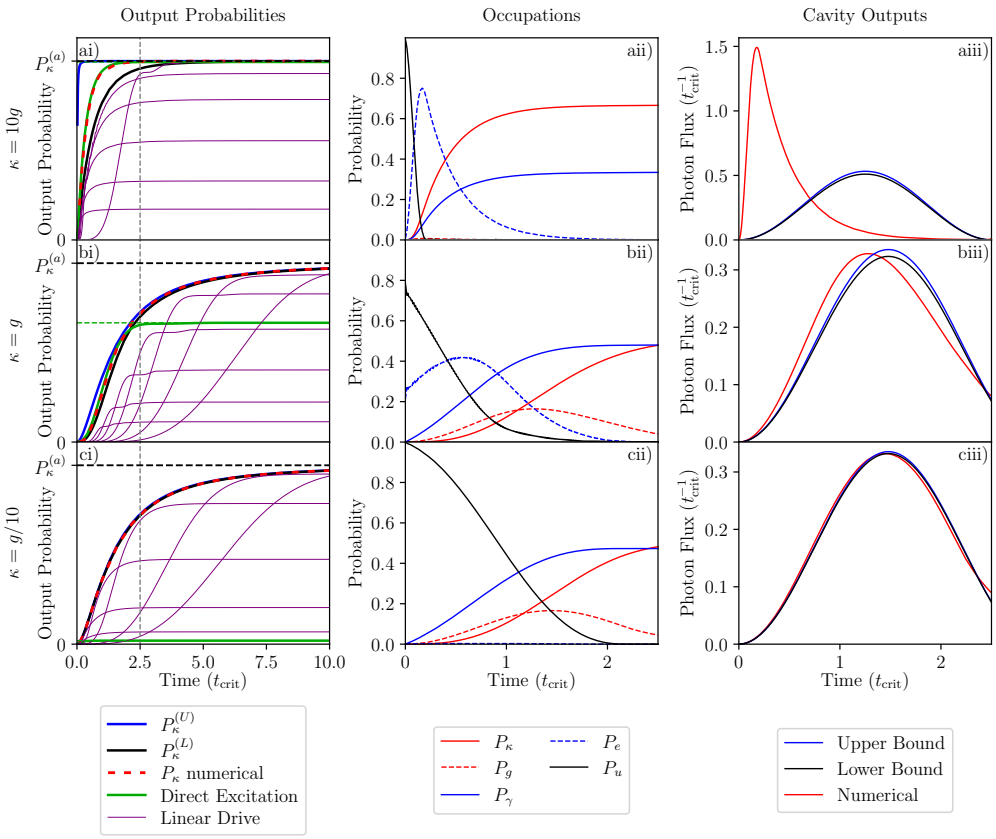

Fig. 3. Comparison of the numerically-optimised performance and analytical performance bounds of Λ-systems with $C = 1$ and row a) $\kappa = 10g$, row b) $\kappa = g$, and row c) $\kappa = g/10$. Column i) Output probabilities achieved through a range of methods against extraction time T. The blue and black lines mark the upper and lower bounds for the maximised extraction probability found in Sec. 2.2 respectively. The red dashed line shows the numerically optimised output. The green line shows the extracted probability for direct excitation to the excited state, with the green dotted line marking the infinite-time extraction probability from direct excitation $P_\kappa^{(e)}$ (Eq. (36)). The purple lines show the output for a series of drives with linearly increasing amplitude and $\Delta_u = 0$, where the rate of increase of drive amplitude is varied between different lines. The adiabatic extraction probability $P_\kappa^{(a)}$ (Eq. (1)) is marked by the dotted black line, and takes a value of 2/3 for all scenarios. The example time used for analysing the system populations and photon wavepackets in ii) and iii) is $T = 2.5/t_{\rm crit}$, and is marked by the grey vertical line. Column ii) System populations for the numerically optimised solution for output time $T = 2.5/t_{\rm crit}$. Column iii) The probability flux of the output wavepackets for the numerically optimised case (red) compared to the upper (black) and lower (blue) bounds.

To probe the variation in optimum wavepacket shape, the optimised wavepacket was calculated at $T = 2.5/t_{\text{crit}}$ for a variety of κ:g ratios, with the results shown in Fig. 4. This shows that, in the limit $g \gg \kappa$, the optimised wavepackets tend to a single shape (when viewed in units normalised to t_{crit}). This is because, for $g > \kappa$, Eq. (18) always predicts the same upper bound in the normalised units, and the optimised wavepacket is very similar to this upper bound. However, as κ/g increases, there is a gradual transition in shape towards the limit $\kappa \gg g$, which features a fast rise followed by a prolonged exponential decay. Profiles in the regime $\kappa > g$ also feature much more pronounced excited state occupations, which was also observed in [30].

To understand why significant excited state population would distort the optimised wavepacket from the sinusoidal shape, it is important to remember that this shape was derived from the upper bound probability condition that $P_\kappa(T)+P_\gamma(T)+P_g(T) = 1$. The optimised wavepacket will only deviate from the upper bound shape if the true probability condition (that $P_\kappa(t) + P_\gamma(t) + P_g(t) + P_e(t) = 1 - P_u(t) = 1$ for some time t during the process) is not equivalent to the upper bound condition. This requires either that $P_e(T) \neq 0$, or that $P_u(t)$ reaches zero at an intermediate time, which, given that $P_\kappa(t)$ and $P_\gamma(t)$ are monotonically increasing, would imply significant P_e or P_g at this intermediate time.

Observing the presented data again, we can broadly classify the observed profiles into two sets. For one set (Fig. 4e), $P_u(t)$ tends smoothly towards zero at T and the output approximates a sinusoidal profile. In the other set (Fig. 4b, c, and d), $P_u(t)$ reaches zero at an intermediate time, and the output wavepacket features an exponential tail from this time onwards, indicated by the shape of the blue panes below the line in Fig. 4a). Thus, for these cases, the probability condition is not a single restriction at the final time, but a continuous restriction for all later times. Therefore, in the $g \gg \kappa$ limit of the data, the dynamics are constrained by probabilities at the final time T, and are consequently dominated by the monotonically increasing probabilities P_κ and P_γ. However, in the $\kappa \gg g$ limit, the dynamics are constrained by the probability sum condition over a period of times, meaning that the undulating probabilities P_g and P_e play an important role, and the shape derived in Sec. 2.2 is not a good approximation.

In summary then, the upper bound is easily calculable, but is not physically realisable, either because $P_e(T)$ is not exactly zero as assumed in the probability condition Eq. (8), or the total probability not in the initial state would have to exceed unity at some point during the process. The lower bound is physically realisable, but it has an assumed, rather than optimum shape. The numeric method can find the wavepacket shape that optimises the output probability (which must lie between the bounds), however the wavepacket shape can be substantially different from that of the bounds. This optimum wavepacket shape can provide considerably reduced photon durations compared to simple linear drives operating at the same extraction efficiency, but the magnitude of this improvement depends strongly of the cavity parameter regime.

Finally, we note that the slight high-frequency noise seen in certain profiles (most obviously in Fig. 3bii) is likely a numerical artefact rather than a genuine feature. See Supplement 1 Sec. 5 for more details.

4.2. Optimisation of probability metrics

The numeric method of Sec. 3 is able to model emitter systems with multiple emitter-occupied cavity states, which is a common scenario for atomic emitters. Fig. 5 shows how a single emitter-cavity system can be used to optimise different outputs. Here we take a system with $\gamma = 0.6\kappa$ and three emitter-occupied cavity states, such that $g_1 = \sqrt{1/3}\,\kappa$, $g_2 = -\sqrt{4/15}\,\kappa$, and $g_3 = \sqrt{1/30}\,\kappa$, which matches the example of an atomic $D_{\frac{5}{2}} \rightarrow P_{\frac{3}{2}}$ transition, where the initial state has angular momentum projection $m_J = 3/2$ along the magnetic field and the cavity is oriented orthogonal to the magnetic field. The energy splitting between emitter-occupied cavity states is 5κ. The driving of this system was optimised for both strong single photon emission paths independently, P_{κ_1} for row a) and P_{κ_2} for row b), and the two-component decay probability

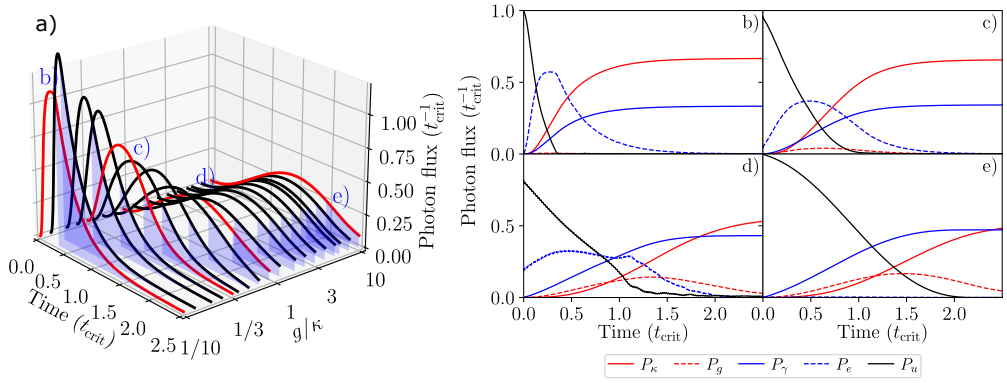

Fig. 4. Comparison of optimised cavity output profile as a function of Λ-system parameters. a) A collection of optimised output wavepackets found as the ratio of g to κ is varied, with γ adjusted to maintain the cooperativity $C = 1$, and the photon collection time set to $2.5t_{\text{crit}}$ for all data. The first time at which $P_u(t)$ is reduced below 1% is marked by the beginning of the blue pane under each curve. Profiles taken as case studies are drawn with red lines, and are labelled in blue according to their corresponding probability panel. b)-e): System probabilities as a function of time for the corresponding output profiles labelled in a).

$P_{\kappa_1} P_{\kappa_2}$, pertinent for protocols where emitter-photon correlations are desired, in row c). Note that this two-component probability product is not a two-photon event, but a maximisation of a product of two probabilities related to single photon emission. It should also be noted that, for the example cavity geometry and transitions, the photon-occupied states $|1_1\rangle$ and $|1_3\rangle$ would be identical (and $|1_2\rangle$ would have the orthogonal polarisation). This means that, while it is possible to distinguish P_{κ_1} and P_{κ_3} with an emitter measurement (justifying that they are distinct probabilities), it is not possible to distinguish them by photonic measurement. This must be understood when applying these methods to schemes where emitter measurement is not possible, for example remote entanglement schemes [13] where emitter measurement would destroy the intended entanglement.

The results show that the same cavity system can be used to produce relatively pure single photon emission through either strong decay channel, or a binary emitter-photon correlated state through changing the driving pulse. However, while the single probability-optimised scenarios (rows a and b) produce smooth wavepackets, the probability product-optimised wavepacket (row c) features significant oscillations. If the system were driven with the typical bichromatic drive [49], then these oscillations would be attributed to off-resonant coupling between one drive tone and the 'opposite' transition. However, our optimisation does not assume a specific form of driving pulse. We therefore see that it is not possible to produce non-undulating wavepackets without compromising on output probability. Finally, it should be noted that the method can optimise more general products or sums of probabilities, a faculty which may be used to discourage unwanted processes that contribute to error in a target application.

4.3. Case study: Effect of ground-state splitting on remote entanglement

Finally, we demonstrate the use of the numeric methods for understanding how emitter structure limits the performance of quantum protocols, taking two-photon, probabilistic, polarisation-encoded remote entanglement as a case study. In these schemes, two separate emitter-cavity systems are driven such that they both produce a single photon whose polarisation qubit is entangled with the final emitter state. For concreteness, we will imagine a system where $|g_1\rangle$ and $|g_2\rangle$ form the emitter qubit, and $|1_1\rangle$ and $|1_2\rangle$ have orthogonal polarisations so that the output

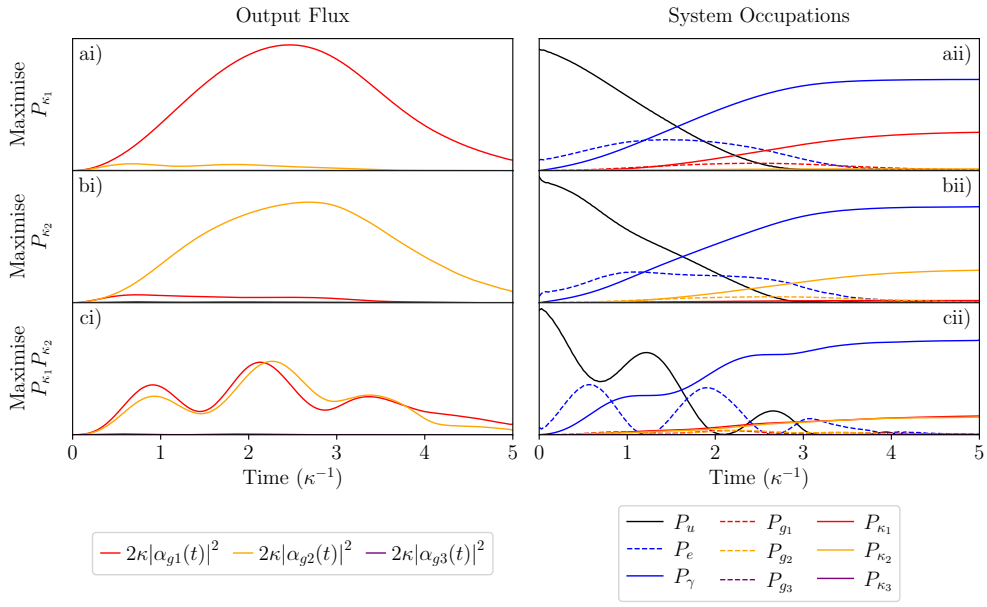

Fig. 5. Example photon wavepackets (Column i) and system populations (Column ii) that maximise different probabilities for an emitter cavity system with $g_1 = \sqrt{1/3}\kappa$, $g_2 = -\sqrt{4/15}\kappa$, $g_3 = \sqrt{1/30}\kappa$, and $\gamma = 0.6\kappa$ over a time of $T = 5/\kappa$. The energy splitting between $|g_1, 1_1\rangle$ and $|g_2, 1_2\rangle$, and $|g_2, 1_2\rangle$ and $|g_3, 1_3\rangle$, is 5κ. Row a) shows the case where the maximised quantity is the single photon emission probability P_{κ_1}, row b) P_{κ_2}, and row c) the two-probability product $P_{\kappa_1}P_{\kappa_2}$.

wavepackets collectively constitute a polarisation qubit. The photon wavepackets from the two systems are routed to opposite input ports of a non-polarising beamsplitter and then subject to polarisation-resolved measurement. Upon certain outcomes of this measurement, the emitters are entangled (see [13, 31] for more details of the scheme). Assuming two identical emitter-cavity systems are used, the probability of remote entanglement success in a given trial is proportional to $P_{\kappa_1}P_{\kappa_2}$ [50]. Even state-of-the-art free space [51] and cavity-enhanced [41] experimental implementations have success probability well below unity, leading to remote entanglement far slower than local operations, inhibiting the protocol's current usefulness. Given the importance of success probability and rate, it is crucial to understand exactly how different experimental parameters affect these quantities.

In an experimental scenario, the two pertinent emitter-occupied cavity states are not typically degenerate, with the splitting potentially chosen for reasons not directly related to the entanglement generation process. It is therefore of interest to know what impact a splitting (denoted Δ_Z as it would often constitute a Zeeman splitting in atom or ion applications) would have on the remote entanglement success probability.

We thus maximise $P_{\kappa_1}P_{\kappa_2}$ as a function of emitter-occupied cavity statesplitting Δ_Z and output time T for the system investigated in Sec. 4.2, but where the third emitter-occupied cavity state has been removed for simplicity. The results are shown in Fig. 6, which shows broadly that an increasing emitter-occupied cavity state splitting reduces the optimised remote entanglement success probability, with a high probability plateau for small Δ_Z, a low plateau for large Δ_z, and a transition in between.

Simple pictures for the limiting cases of photon extraction in limited time with $\Delta_Z = 0$ and $\Delta_Z \to \infty$ can be used to understand the dependence of $P_{\kappa_1}P_{\kappa_2}$ on Δ_Z, with derivations for these limits given in Supplement 1 Sec. 6. Firstly, in the case of $\Delta_Z = 0$, the two decay channels have

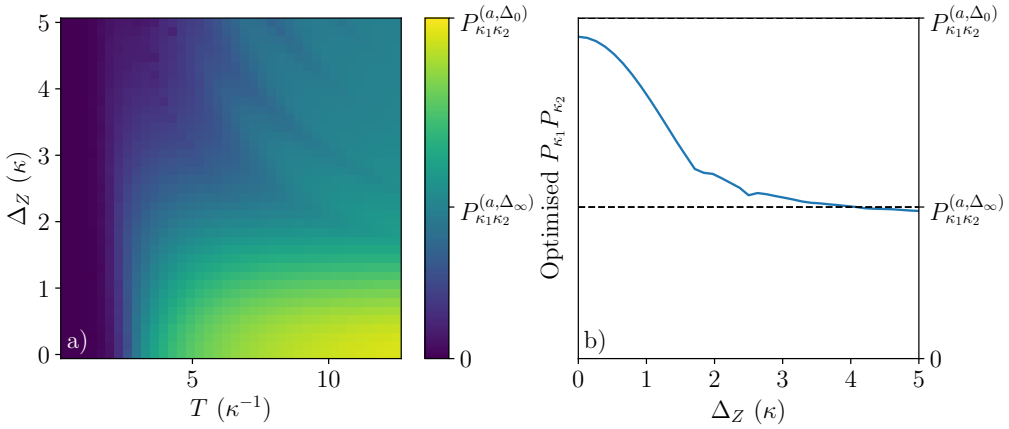

Fig. 6. Investigation of the effect of ground state splitting Δ_Z on the two-component probability $P_{\kappa_1}P_{\kappa_2}$ optimised for time T for a system with $g_1 = \sqrt{1/3}\kappa$, $g_2 = -\sqrt{4/15}\kappa$ and $\gamma = 0.6\kappa$. a) The optimised $P_{\kappa_1}P_{\kappa_2}$ as a function of T and Δ_Z. b) The optimised output probability as a function of Δ_Z for just the longest time shown ($T = 12.5/\kappa$) compared to the expected infinite time output for zero-splitting case $P^{(a,\Delta_0)}_{\kappa_1\kappa_2}$ and for the high-splitting case $P^{(a,\Delta_\infty)}_{\kappa_1\kappa_2}$.

no differential phase evolution, so the excited state actually couples directly to a single level with rate $g_{\text{eff}} = \sqrt{g_1^2 + g_2^2}$. This results in the infinite-time probability product

$$P^{(a,\Delta_0)}_{\kappa_1\kappa_2} = \frac{g_1^2 g_2^2}{g_{\text{eff}}^4}\left(\frac{g_{\text{eff}}^2}{g_{\text{eff}}^2 + \kappa\gamma}\right)^2. \tag{37}$$

Secondly, in the case that the Zeeman splitting becomes large, the production processes for the two components should be spectrally decoupled. This leads to an optimised $P_{\kappa_1}P_{\kappa_2}$ of

$$P^{(a,\Delta_\infty)}_{\kappa_1\kappa_2} = \frac{2C_1 2C_2}{4(2C_1+1)(2C_2+1)}. \tag{38}$$

The agreement of the data with Eqs. (37) and (38) is shown in panel b) of Fig. 6. The data does not extend to infinite extraction time T, or to infinite state splitting Δ_Z, but the trend broadly matches the values expected from these simple models.

While the conclusions of Fig. 6 are not themselves surprising, it is worth emphasising the key advantage of the optimisation method: that it is driving-independent. This means that we attribute the reduction in success probability with Δ_Z directly to the increase in Δ_Z, without any doubt about whether we chose unsuitable driving pulses for some parameters. The same procedure could be applied to understand the dependence upon system parameters of the success probability of other quantum information protocols.

5. Conclusions

We have developed an analytic method to establish upper and lower bounds to the probability of photon extraction from a Λ-system in finite time which lie within the previously known infinite time bounds. We then extended these ideas to establish a numeric method to find the limits to photon extraction which also applies to generalisations of the Λ-system to include multiple cavity decays. This method can optimise general probability products, and, in-keeping with recent developments for related problems [28, 30], does so without optimising the driving

pulse explicitly. The combination of these approaches allows us to calculate the limits to the compromise between photon extraction probability and rate, and investigate optimised output wavepackets and corresponding quantum dynamics.

For the canonical Λ-system, we find the photon wavepacket which maximises finite-time photon extraction probability for given system parameters, observing that its shape lies on a spectrum between the exponential decay characteristic of fast excitation and the sinusoidal profile of the analytic bounds, and that this wavepacket can result in significantly faster high-efficiency photon extraction compared to simple driving approaches. In the case of generalised Λ-systems, which are often more accurate models of real experiments, we observed how to determine the limits of a single system, taken to model a trapped ion-cavity system, in producing single photons of specified polarisation, or an emitter photon correlated state. We then demonstrated how our methods can be used to derive driving-independent conclusions about the impact of system parameters, exemplified by the reduction of remote entanglement success probability with increasing emitter-occupied cavity state splitting.

We believe that the methods presented in this manuscript will aid researchers in realising high-rate high-efficiency cavity-based sources for single photons and emitter-photon entangled states across the development cycle. Firstly, the methods determine the performance limits of existing hardware and how they can be reached. This specifically accounts for the finite protocol duration and extra emitter structure seen in experimental attempts to reach these limits [21]. Secondly, the approach can reveal how the parameters of future systems will affect their performance, enabling the targeting of designs towards high performance use, which would again allow for the photon production time to be properly included in place of infinite time results [52]. Finally, the advantages of our driving-independent approach are complementary to that of optimal control, and the combination of the two may help identify robust driving schemes with near-ideal performance in practical systems. Additionally, we also reiterate that photon emission is deeply related to photon absorption, and our results in the context of photon emission experiments have direct analogues for the applications requiring finite-time absorption of photon wavepackets.

6. Backmatter

Funding. This work was funded by the UK Engineering and Physical Sciences Research Council Hub in Quantum Computing and Simulation (EP/T001062/1), the UK Research and Innovation Frontier Research Fellowship (ERC Guarantee) MICRON-QC (EP/Y026438/1), and the European Union Quantum Technology Flagship Project AQTION (No. 820495).

Acknowledgments. The authors acknowledge the use of the IRIDIS High Performance Computing Facility, and associated support services at the University of Southampton, in the completion of this work. The authors would like to thank Dr. Thomas Doherty at the University of Oxford for careful reading of and insightful comments on this manuscript.

Disclosures. The authors declare no conflicts of interest.

Data Availability Statement. Data underlying the results presented in this paper are available in Ref. [53].

Supplemental document. See Supplement 1 for supporting content.

References

1. C. J. Hood, M. S. Chapman, T. W. Lynn, and H. J. Kimble, "Real-time cavity qed with single atoms," Phys. Rev. Lett. **80**, 4157–4160 (1998).
2. K. M. Birnbaum, A. Boca, R. Miller, *et al.*, "Photon blockade in an optical cavity with one trapped atom," Nature **436**, 87–90 (2005).
3. B. Casabone, K. Friebe, B. Brandstätter, *et al.*, "Enhanced quantum interface with collective ion-cavity coupling," Phys. Rev. Lett. **114**, 023602 (2015).

4. T. Stolz, H. Hegels, M. Winter, *et al.*, "Quantum-logic gate between two optical photons with an average efficiency above 40%," Phys. Rev. X **12**, 021035 (2022).
5. B. Casabone, A. Stute, K. Friebe, *et al.*, "Heralded entanglement of two ions in an optical cavity," Phys. Rev. Lett. **111**, 100505 (2013).
6. F. Haas, J. Volz, R. Gehr, *et al.*, "Entangled states of more than 40 atoms in an optical fiber cavity," Science **344**, 180–183 (2014).
7. J. Ramette, J. Sinclair, Z. Vendeiro, *et al.*, "Any-to-any connected cavity-mediated architecture for quantum computing with trapped ions or rydberg arrays," PRX Quantum **3**, 010344 (2022).
8. A. Holleczek, O. Barter, A. Rubenok, *et al.*, "Quantum logic with cavity photons from single atoms," Phys. Rev. Lett. **117**, 023602 (2016).
9. S. Wehner, D. Elkouss, and R. Hanson, "Quantum internet: A vision for the road ahead," Science **362**, eaam9288 (2018).
10. A. Reiserer, "Colloquium: Cavity-enhanced quantum network nodes," Rev. Mod. Phys. **94**, 041003 (2022).
11. C. Monroe, R. Raussendorf, A. Ruthven, *et al.*, "Large-scale modular quantum-computer architecture with atomic memory and photonic interconnects," Phys. Rev. A **89**, 022317 (2014).
12. C. Cabrillo, J. I. Cirac, P. García-Fernández, and P. Zoller, "Creation of entangled states of distant atoms by interference," Phys. Rev. A **59**, 1025–1033 (1999).
13. C. Simon and W. T. M. Irvine, "Robust long-distance entanglement and a loophole-free bell test with ions and photons," Phys. Rev. Lett. **91**, 110405 (2003).
14. S. Ritter, C. Nölleke, C. Hahn, *et al.*, "An elementary quantum network of single atoms in optical cavities," Nature **484**, 195–200 (2012).
15. J. Bochmann, M. Mücke, G. Langfahl-Klabes, *et al.*, "Fast excitation and photon emission of a single-atom-cavity system," Phys. Rev. Lett. **101**, 223601 (2008).
16. H. Goto, S. Mizukami, Y. Tokunaga, and T. Aoki, "Figure of merit for single-photon generation based on cavity quantum electrodynamics," Phys. Rev. A **99**, 053843 (2019).
17. C. K. Law and H. J. Kimble, "Deterministic generation of a bit-stream of single-photon pulses," J. Mod. Opt. **44**, 2067–2074 (1997).
18. G. S. Vasilev, D. Ljunggren, and A. Kuhn, "Single photons made-to-measure," New J. Phys. **12**, 063024 (2010).
19. C. Maurer, C. Becher, C. Russo, *et al.*, "A single-photon source based on a single ca+ ion," New J. Phys. **6**, 94 (2004).
20. A. Stute, B. Casabone, P. Schindler, *et al.*, "Tunable ion-photon entanglement in an optical cavity," Nature **485**, 482–485 (2012).
21. J. Schupp, V. Krcmarsky, V. Krutyanskiy, *et al.*, "Interface between trapped-ion qubits and traveling photons with close-to-optimal efficiency," PRX Quantum **2**, 020331 (2021).
22. A. Kuhn, M. Hennrich, T. Bondo, and G. Rempe, "Controlled generation of single photons from a strongly coupled atom-cavity system," Appl. Phys. B **69**, 373–377 (1999).
23. A. Kuhn, M. Hennrich, and G. Rempe, "Deterministic single-photon source for distributed quantum networking," Phys. Rev. Lett. **89**, 067901 (2002).
24. H. G. Barros, A. Stute, T. E. Northup, *et al.*, "Deterministic single-photon source from a single ion," New J. Phys. **11**, 103004 (2009).
25. M. Hennrich, T. Legero, A. Kuhn, and G. Rempe, "Vacuum-stimulated raman scattering based on adiabatic passage in a high-finesse optical cavity," Phys. Rev. Lett. **85**, 4872–4875 (2000).
26. C. Monroe and J. Kim, "Scaling the ion trap quantum processor," Science **339**, 1164–1169 (2013).
27. P. Drmota, D. Main, D. P. Nadlinger, *et al.*, "Robust quantum memory in a trapped-ion quantum network node," Phys. Rev. Lett. **130**, 090803 (2023).
28. B. Tissot and G. Burkard, "Efficient high-fidelity flying qubit shaping," Phys. Rev. Res. **6**, 013150 (2024).
29. T. Ward and M. Keller, "Generation of time-bin-encoded photons in an ion-cavity system," New J. Phys. **24**, 123028 (2022).
30. T. Utsugi, A. Goban, Y. Tokunaga, *et al.*, "Gaussian-wave-packet model for single-photon generation based on cavity quantum electrodynamics under adiabatic and nonadiabatic conditions," Phys. Rev. A **106**, 023712 (2022).
31. L. Luo, D. Hayes, T. Manning, *et al.*, "Protocols and techniques for a scalable atom–photon quantum network," Fortschr. Phys. **57**, 1133–1152 (2009).
32. M. Mücke, J. Bochmann, C. Hahn, *et al.*, "Generation of single photons from an atom-cavity system," Phys. Rev. A **87**, 063805 (2013).
33. J. O. Ernst, J. R. Alvarez, T. D. Barrett, and A. Kuhn, "Bursts of polarised single photons from atom-cavity sources," J. Phys. B: At. Mol. Opt. Phys. **56**, 205003 (2023).
34. J. I. Cirac, P. Zoller, H. J. Kimble, and H. Mabuchi, "Quantum state transfer and entanglement distribution among distant nodes in a quantum network," Phys. Rev. Lett. **78**, 3221–3224 (1997).
35. A. V. Gorshkov, A. André, M. D. Lukin, and A. S. Sørensen, "Photon storage in Λ-type optically dense atomic media. ii. free-space model," Phys. Rev. A **76**, 033805 (2007).
36. A. V. Gorshkov, A. André, M. D. Lukin, and A. S. Sørensen, "Photon storage in Λ-type optically dense atomic media. i. cavity model," Phys. Rev. A **76**, 033804 (2007).
37. J. Dilley, P. Nisbet-Jones, B. W. Shore, and A. Kuhn, "Single-photon absorption in coupled atom-cavity systems," Phys. Rev. A **85**, 023834 (2012).

38. L. Giannelli, T. Schmit, T. Calarco, *et al.*, "Optimal storage of a single photon by a single intra-cavity atom," New J. Phys. **20**, 105009 (2018).
39. K. A. Fischer, L. Hanschke, J. Wierzbowski, *et al.*, "Signatures of two-photon pulses from a quantum two-level system," Nat. Phys. **13**, 649–654 (2017).
40. M. Meraner, A. Mazloom, V. Krutyanskiy, *et al.*, "Indistinguishable photons from a trapped-ion quantum network node," Phys. Rev. A **102**, 052614 (2020).
41. V. Krutyanskiy, M. Galli, V. Krcmarsky, *et al.*, "Entanglement of trapped-ion qubits separated by 230 meters," Phys. Rev. Lett. **130**, 050803 (2023).
42. T. Walker, S. V. Kashanian, T. Ward, and M. Keller, "Improving the indistinguishability of single photons from an ion-cavity system," Phys. Rev. A **102**, 032616 (2020).
43. S. Kikura, R. Asaoka, M. Koashi, and Y. Tokunaga, "High-purity single-photon generation based on cavity qed," arXiv preprint arXiv:2403.00072 (2024).
44. T. D. Barrett, D. Stuart, O. Barter, and A. Kuhn, "Nonlinear zeeman effects in the cavity-enhanced emission of polarised photons," New J. Phys. **20**, 073030 (2018).
45. T. Wilk, S. C. Webster, A. Kuhn, and G. Rempe, "Single-atom single-photon quantum interface," Science **317**, 488–490 (2007).
46. P. P. Rohde, T. C. Ralph, and M. A. Nielsen, "Optimal photons for quantum-information processing," Phys. Rev. A **72**, 052332 (2005).
47. O. Morin, M. Körber, S. Langenfeld, and G. Rempe, "Deterministic shaping and reshaping of single-photon temporal wave functions," Phys. Rev. Lett. **123**, 133602 (2019).
48. G. Cui and M. G. Raymer, "Quantum efficiency of single-photon sources in the cavity-qed strong-coupling regime," Opt. Express **13**, 9660–9665 (2005).
49. A. Stute, B. Casabone, B. Brandstätter, *et al.*, "Toward an ion-photon quantum interface in an optical cavity," Appl. Phys. B: Lasers Opt. **107**, 1145–1157 (2012).
50. D. L. Moehring, P. Maunz, S. Olmschenk, *et al.*, "Entanglement of single-atom quantum bits at a distance," Nature **449**, 68–71 (2007).
51. D. P. Nadlinger, P. Drmota, B. C. Nichol, *et al.*, "Experimental quantum key distribution certified by bell's theorem," Nature **607**, 682–686 (2022).
52. S. Gao, J. A. Blackmore, W. J. Hughes, *et al.*, "Optimization of scalable ion-cavity interfaces for quantum photonic networks," Phys. Rev. Appl. **19**, 014033 (2023).
53. W. J. Hughes, J. F. Goodwin, and P. Horak, "Dataset: Optimising finite-time photon extraction from emitter-cavity systems," (2024). doi: https://doi.org/10.5258/SOTON/D3091.